Review of Scientific Instruments

RESEARCH ARTICLE | MARCH 04 2024

A device for magnetic-field angle control in magneto-optical filters using a solenoid-permanent magnet pair

Sharaa A. Alqarni ; Jack D. Briscoe ; Clare R. Higgins ; Fraser D. Logue ; Danielle Pizzey ; Thomas G. Robertson-Brown ; Ifan G. Hughes

Rev. Sci. Instrum. 95, 035103 (2024)
https://doi.org/10.1063/5.0174264

AIP Publishing

Review of Scientific Instruments ARTICLE pubs.aip.org/aip/rsi

A device for magnetic-field angle control in magneto-optical filters using a solenoid-permanent magnet pair

Cite as: Rev. Sci. Instrum. 95, 035103 (2024); doi: 10.1063/5.0174264
Submitted: 29 August 2023 • Accepted: 7 February 2024 •
Published Online: 4 March 2024

Sharaa A. Alqarni,[a),b)] Jack D. Briscoe, Clare R. Higgins, Fraser D. Logue, Danielle Pizzey, Thomas G. Robertson-Brown,[c)] and Ifan G. Hughes

AFFILIATIONS

Department of Physics, Durham University, South Road, Durham DH1 3LE, United Kingdom

[a)] **Author to whom correspondence should be addressed:** sharaa.alqarni@durham.ac.uk
[b)] **Also at:** Department of Physics, College of Sciences and Arts, Najran University, Najran, Saudi Arabia
[c)] **Also at:** Department of Physics, Swansea University, Swansea, United Kingdom

ABSTRACT

Atomic bandpass filters are used in a variety of applications due to their narrow bandwidths and high transmission at specific frequencies. Predominantly, these filters are in the Faraday (Voigt) geometry, using an applied axial (transverse) magnetic field with respect to the laser propagation direction. Recently, there has been interest in filters realized with arbitrary-angle magnetic fields, which have been made by rotating permanent magnets with respect to the *k*-vector of the interrogating laser beam. However, the magnetic field angle achievable with this method is limited as field uniformity across the cell decreases as the rotation angle increases. In this work, we propose and demonstrate a new method of generating an arbitrary-angle magnetic field, using a solenoid to produce a small, and easily alterable, axial field, in conjunction with fixed permanent magnets to produce a large transverse field. We directly measure the fields produced by both methods, finding them to be very similar over the length of the vapor cell. We then compare the transmission profiles of filters produced using both methods, again finding excellent agreement. Finally, we demonstrate the sensitivity of the filter profile to changing magnetic field angle (solenoid current), which becomes easier to exploit with the much improved angle control and precision offered by our new design.

I. INTRODUCTION

Narrowband magneto-optical bandpass filters[1–7] find great utility across a range of disciplines, including solar monitoring,[8–12] atmospheric LIDAR,[13–15] and intra-cavity laser frequency stabilization.[16–19] The spectrum of the light transmitted through an atomic vapor cell subjected to an external magnetic field is dependent on the relative orientation of the magnetic field and the *k*-vector of the light. The most commonly used geometries are the Faraday configuration,[20–22] where the magnetic field is parallel to the *k*-vector of the interrogating light, and the Voigt configuration,[23] where the magnetic field is perpendicular to the *k*-vector.[24–32] The general case with an arbitrary angle between the magnetic field and the axis of propagation is more difficult to treat mathematically—and to optimize experimentally—as the working angular range of the magneto-optical filter is limited, and slight deviations from the optimum angle lead to reduced filter efficiency and spectral distortion. Consequently, there are far fewer experimental studies of this case owing to difficulties in setting and controlling the magnetic field angle without encroaching on line-of-sight propagation.[33–35] Nevertheless, there has been a recent burgeoning interest in this geometry, as it offers the possibility of realizing better magneto-optical filters when compared to Faraday and Voigt geometries.[35,36] In particular, the arbitrary angles that have, to date, provided the best single pass magneto-optical filter performance are within the range 80°–90° with a magnetic field magnitude of several hundred Gauss;[36–38] this is why we have optimized our device to operate within this parameter range. Ongoing research and development efforts aim to address the experimental challenges and improve the performance, stability, and cost-effectiveness of these devices.

In our previous work involving arbitrary-angle filters,[36] the vapor cell length was 5 mm, and the magnetic field was controlled using a pair of permanent magnets positioned on either side of the vapor cell, such as those used in a Voigt geometry setup, but rotated relative to the beam axis. The field strength was set by the magnet

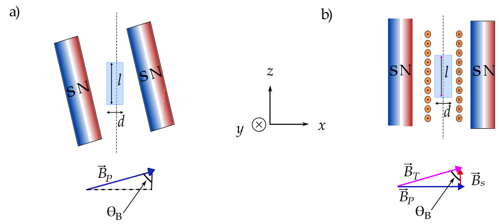

FIG. 1. An arbitrary magnetic field angle with respect to the axis of the laser beam (i.e., along *z*), represented by the vertical, black, dashed line, can be produced by either: (a) a Voigt magnetic field ($\vec{B_{\mathrm{P}}}$) setup rotated by θ_B about the *y*-axis, as shown by the blue vector arrow; or (b) a fixed Voigt magnetic field ($\vec{B_{\mathrm{P}}}$, blue arrow) and a tunable solenoid magnetic field ($\vec{B_{\mathrm{S}}}$, red arrow) produce a combined magnetic field ($\vec{B_{\mathrm{T}}}$, pink arrow) at an angle of θ_B with respect to the *z*-axis. The red–blue rectangles represent a N–S permanent magnet, while the orange circles represent the solenoid, with either a dot or cross showing the current direction. The light blue rectangle shown in the center of the magnet arrangements represents a cylindrical atomic vapor cell of length *l* and diameter *d*.

remanence field and separation, while the angle was set by physically rotating the magnets with respect to the *k*-vector of the laser beam; this concept is illustrated in Fig. 1(a).

Maintaining magnetic field homogeneity at the 1% level and a magnetic field angle θ_B to better than 1° over millimeter vapor cell length scales is trivial,[39] but the use of these short cells comes at the expense of the requirement of elevated operating temperatures to produce sufficient atomic vapor density; this leads to self-broadening of spectral lines[40] and ultimately reduced magneto-optical filter performance.[41] With open-source magnetic field computation programs[42] becoming readily available, designing bespoke magnetic field profiles with field and θ_B homogeneity extending tens of millimeters is now feasible,[43] meaning standard "off-the-shelf" vapor cells—with a length of tens of millimeters—can be used, with correspondingly lower operating temperatures required. Nevertheless, the challenge persists in precisely *aligning* the magnetic field vector with the *k*-vector of the laser beam along the atomic interaction lengthscale—defined by the vapor cell's length. This complexity becomes more pronounced when setting up the filter and employing mirror mounts with three-axis control to guide the laser beam. A longer vapor cell requires precise alignment over longer lengthscales, and a longer cell may obstruct a pair of permanent magnets when they are rotated; consequently, there is a physical limit set on the angular range of an arbitrary-angle filter that utilizes permanent magnets. The longer the cell is, the greater this limitation becomes. While custom hardware solutions can be crafted to establish a static alignment between the laser beam axis and the magnetic field vector at the optimal angle, this approach has its drawbacks. It sacrifices tunability and confines the setup to a fixed set of filter operating parameters.

To address these challenges, we suggest and implement an alternative approach to generate an arbitrary magnetic field angle while maintaining the same field strength. Our approach involves incorporating an air-core solenoid between a pair of Voigt geometry permanent magnets that generate a strong transverse magnetic field, with the vapor cell seated within the bore of the solenoid. A weak axial magnetic field is generated by the solenoid, and the magnitude of this field, and, therefore, the angle of the total field can be regulated by controlling the current. This concept is illustrated in Fig. 1(b).

In this paper, we demonstrate that this combination of Voigt-geometry permanent magnets and a Faraday-geometry solenoid effectively addresses the experimental challenges associated with precise control of small magnetic field angles. Throughout the paper, we will refer to this new method as "solenoid-plus-permanent" and the old method as "rotated-permanent."

The remainder of the paper is organized as follows: in Sec. II, we explain the requirements of the magneto-optical filter and how we come to realize the parameters; in Sec. III, we present the magnetic field computation and compare the rotated-permanent and solenoid-plus-permanent configurations; in Sec. IV, we present measurements of the magnetic field using a Hall probe for the two geometries and compare the filter performance of each; and finally, conclusions are drawn and an outlook is provided in Sec. V.

II. REQUIREMENTS OF THE MAGNETO-OPTICAL FILTER

Figure 2(a-i) illustrates a schematic of the optical apparatus required for a Rb magneto-optical filter and the geometry of the setup, and Fig. 2(b) has photographs of the solenoid-plus-permanent configuration. Light emitted from an external cavity diode (ECD) laser with a center wavelength of 780 nm traverses an optical isolator (OI) and is divided into two separate beams using a polarizing beam-splitter (PBS) and a half-wave retarder plate ($\lambda/2$); one path goes to the magneto-optical filter, the other is for calibration of the frequency axis. Due to the non-linear response of the laser piezo that controls the output frequency, we need to calibrate the laser scan[44,45] so that we can compare our transmission spectrum with the theory. We follow the methods described in Pizzey *et al.*[45] and use a Fabry–Perot etalon for linearization and a 50 mm length natural abundance Rb cell for defining zero-detuning, which is chosen to be the weighted center of the line.[46]

In the magneto-optical filter, the magnetic field vector, along the length of the vapor cell, is oriented in the *x*–*z*-plane at an angle of θ_B to the *z*-axis, where $\theta_B = 0°$ and $\theta_B = 90°$ correspond to the Faraday and Voigt geometries, respectively. The vapor cell is positioned between two high-extinction polarizers [shown in Fig. 2(a-ii)]. The angle between the electric field vector of the light and the *x*-axis, θ_E, influences the coupling between atomic transitions and polarization modes of the light. The angle of the input polarizer, θ_E, can be adjusted, but the relative angle of the two polarizers, GT1 and GT2, remains constant at 90° (i.e., crossed polarizers). This ensures that the transmission is zero in the absence of any atom–light interaction.

Using the open-source computer program *ElecSus*,[47,48] we model the transmission of a weak laser beam[49] through an alkali-metal atomic vapor with a given input polarization, magnetic field strength, and angle. We implement an extension to *ElecSus* to calculate the transmission spectrum of the magneto-optical filter by calculating the subsequent transmission through a polarizer (crossed with respect to the input polarizer) after the vapor cell. A fitting routine can be implemented to optimize the filter peak transmission and linewidth by varying input parameters, such as the vapor temperature, magnetic field strength, and magnetic field angle.

In previous work,[36] optimum magnetic field strength, angle, and atomic vapor temperature were found for a Rb D2 line filter

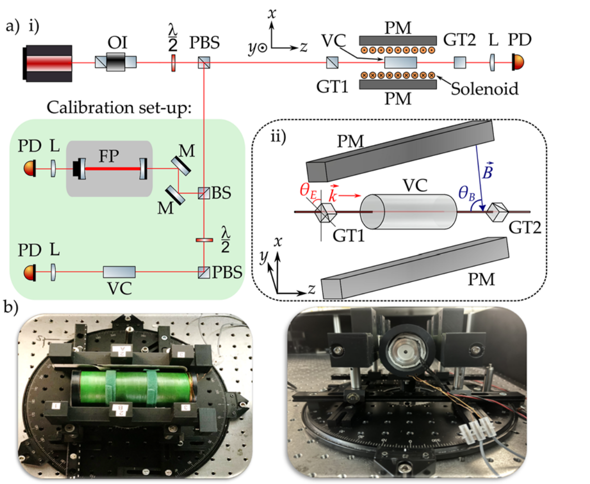

FIG. 2. (a) (i) Schematic of the solenoid-plus-permanent magneto-optical filter setup and geometry. The filter consists of an atomic vapor cell in an applied magnetic field ($\vec{B}$) formed from two rectangular permanent magnets (PM) and a solenoid. The field strength is determined by the separation of the magnets and is adjustable up to 190 G, while the magnetic field angle θ_B is controlled by the current through the solenoid. Shown in the inset (a) (ii) is an illustration of the magnet setup for the rotated-permanent setup. In both methods, the magnetic field is oriented in the x–z-plane at an angle θ_B to the z-axis. An input high-extinction Glan–Taylor polarizer (GT1) is set at an angle θ_E with respect to the x-axis. The output polarizer (GT2) is crossed at 90° to the input polarizer. The transmission of the filter is measured via a lens (L) and a photodetector (PD). In addition, shown is the calibration setup, which includes a Fabry–Pérot etalon (FP) for linearizing the laser scan and a vapor cell (VC) for an absolute frequency reference.[45,54] (b) Photographs showcase the solenoid-plus-permanent magnetic field device positioned on a Thorlabs rotating breadboard, featuring a removable center part that facilitates testing with and without the solenoid in operation. The optics necessary for transforming the device into a filter are not shown. In the top-down view (left), the solenoid, depicted as a green cylinder, is nestled between permanent magnets housed in black containers. The on-axis view (right) reveals the temperature control setup for the vapor cell, utilizing two ceramic heaters. One of these heaters is shown as a white disk with a central hole, allowing the laser beam to pass through the vapor cell.

(natural abundance ratio) using a 5 mm long cell. In this work, however, the magneto-optical filter parameters were not optimized. Instead, the parameters were chosen to work robustly for a vapor cell of length 75 mm since the primary focus of this research is to conduct a comparative analysis between two methods of generating an arbitrary magnetic field rather than fine-tuning the filter parameters for optimal performance. We used *ElecSus* to identify suitable magnetic field parameters, which give a filter profile with a narrow peak and reasonable transmission at line center, for a filter using a l = 75 mm vapor cell. We select a field magnitude of 190 G at an angle, θ_B, of 86°; these parameters also fall within the allowable angle constraints of the rotated-permanent configuration.

We construct a filter with these parameters using the rotated-permanent setup, the normalized transmission of which is shown in Fig. 3. Here, the atomic vapor cell temperature is 368 K. Experimental data are displayed as red points, and an *ElecSus* fit to the data is shown by a solid blue line, with fit parameters as displayed in the figure. Residuals are plotted underneath, showing

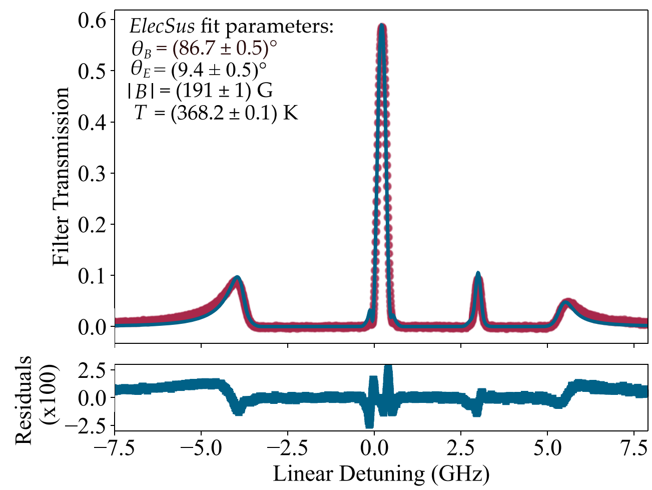

FIG. 3. Experimental transmission (blue data points) as a function of linear detuning of an arbitrary angle magneto-optical filter for a naturally abundant Rb vapor cell of l = 75 mm. The magnetic field angle θ_B was produced by rotating permanent magnets, as shown in Fig. 2(a-ii). A theoretical *ElecSus* fit (red solid line) with corresponding residuals is shown.

very good agreement between theory and experiment. As previously demonstrated,[36,38] we see that the *ElecSus* model describes the magneto-optical filter behavior well, and we will use this later in the work to further test the effectiveness of our new arbitrary-angle-field generation method.

III. ARBITRARY-ANGLE MAGNETIC FIELD CONTROL

We will simulate the magnetic field profiles of two designs—rotated-permanent [Fig. 1(a)] and solenoid-plus-permanent [Fig. 1(b)]—and compare the field homogeneity and tolerances. For the solenoid-plus-permanent configuration to produce a magnetic field angle of $\theta_B = 86°$, we require the solenoid to produce an axial magnetic field of 13 G over a length scale of l = 75 mm.

We use *Magpylib*,[42] an open-source Python package for magnetic field computation, to simulate the magnetic field geometry. To produce the field strength required for the magneto-optical filter discussed in Sec. II, we employed "off-the-shelf" commercially available strontium ferrite permanent magnets of grade Y30BH due to their easy availability. These magnets are cuboidal, measuring 15 × 20 × 60 mm^3 along the x, y, and z axes, respectively. They are magnetized along the x-axis, with each individual magnet having a slightly different strength, with a variation of 5% between the weakest and strongest. To ensure field homogeneity across the 75 mm length of the vapor cell, we stacked three magnets along the z-axis for each half of the setup. This arrangement resulted in a total of six magnets forming the Voigt permanent magnet configuration. 3D printed plastic holders were used, each holding three magnets. A pair of symmetrical holders constituted the Voigt permanent magnet geometry, with the separation of magnets along the x-axis being adjustable. The field strength is determined by the distance between the permanent magnets, which we set to be 74 mm, giving a field strength of $|B|$ = 190 G along the propagation axis ($x = 0, y = 0, z = z'$). The Voigt

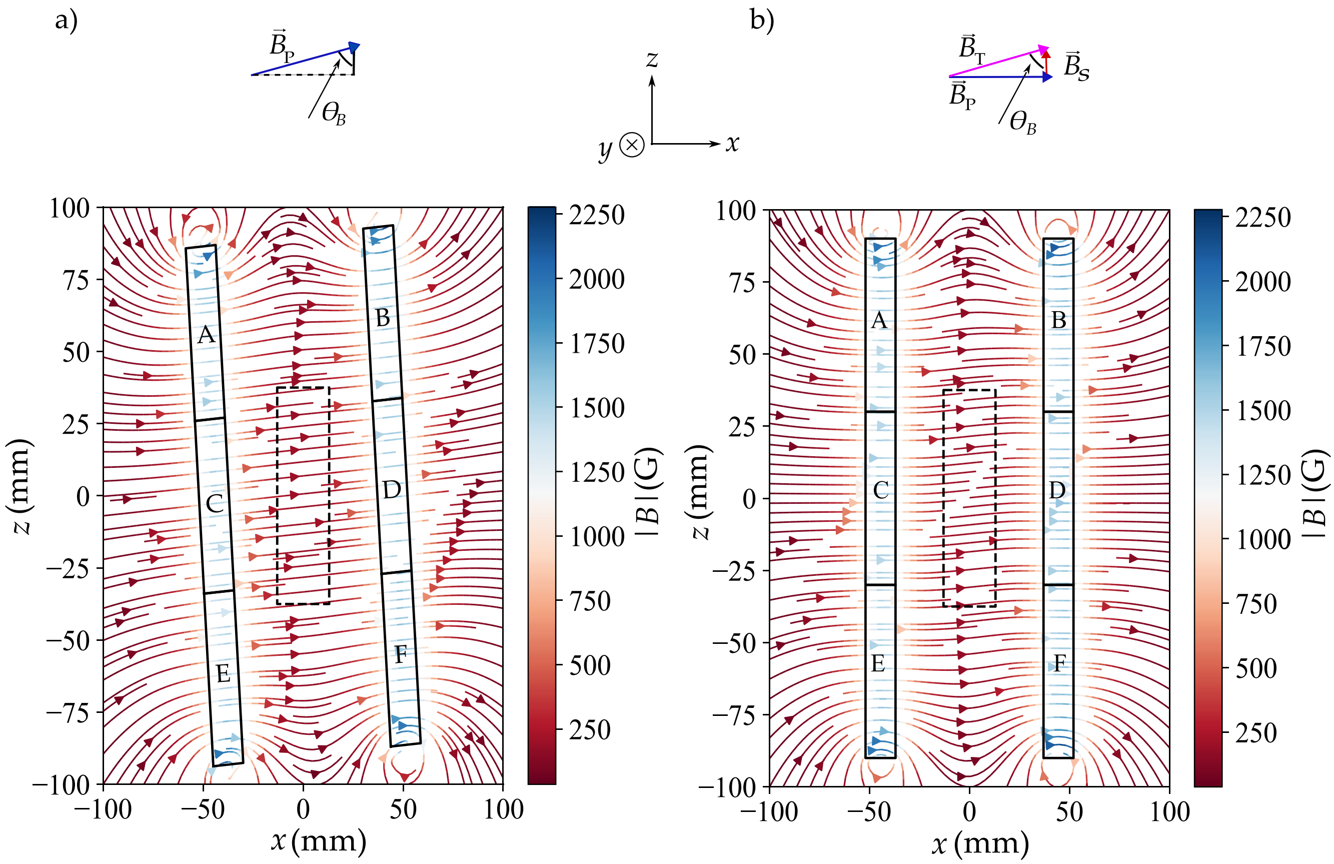

FIG. 4. *Magpylib* magnetic field simulations for the magnetic field configurations shown in Fig. 1 for six permanent magnets labeled A–F. The physical profile of each individual magnet is shown by a black solid line in the contour plots, and the field strengths of each magnet, which vary by 5% between the weakest and strongest, are accounted for in the *Magpylib* model. The arrows indicate the magnetic field vector's direction, while the color and accompanying colorbar represent the magnitude of the magnetic field. (a) rotated-permanent configuration—Voigt permanent magnets rotated by an angle $\theta = 4°$. (b) solenoid-plus-permanent configuration—Voigt configuration permanent magnets and a solenoid current of 525 mA, which generates a *B*-field along *z* of 13 G. The physical profile of the solenoid wires is not displayed in the contour plot.

permanent magnet configuration is mounted on a Thorlabs rotating breadboard featuring a removable center portion (RBB300A/M). This setup enables the vapor cell to remain fixed with respect to the laser beam axis (i.e., z-axis) while allowing for the rotation of the Voigt magnets to generate the desired arbitrary magnetic field angle. Figure 4(a) illustrates the *Magpylib* simulations of the rotated-permanent configuration. The arrows indicate the direction of the magnetic field vectors, while the color and accompanying colorbar illustrate the strength of the field. The black dashed line between the Voigt magnets illustrates the physical profile of the $l = 75$ mm vapor cell.

The solenoid is required to be longer than the length of the vapor cell for magnetic field homogeneity and possess a central bore capable of accommodating both the vapor cell and its heater. In addition, the solenoid should generate an axial magnetic field of 13 G without requiring excessive current to prevent overheating of the solenoid wires. According to *Magpylib* simulations, we established that a solenoid with a length of 140 mm and an inner diameter (ID) of 45 mm, consisting of two layers of 156 turns of wire with a thickness of 0.9 mm, would yield the desired axial field when supplied with less than 1 A of current. The solenoid is formed by winding copper wire around a cylindrical PTFE former of the appropriate dimensions, ensuring thermal isolation between the vapor cell and the solenoid; this allows us to have independent control over the magnetic field and the temperature of the vapor cell. The solenoid is also mounted within the center portion of the rotating breadboard, such that when the Voigt permanent magnets are rotated, the solenoid and vapor cell remain stationary. Figure 4(b) illustrates the *Magpylib* simulations of the solenoid-plus-permanent configuration with a solenoid current of 525 mA. It can be seen that along the z-axis ($x = 0$, $y = 0$), within the z-range of the vapor cell ($+37.5$ mm $> z > -37.5$ mm), the field magnitude and direction of the two configurations are almost identical. This is shown explicitly in the theory lines in Fig. 5.

We also use *Magpylib* to simulate the effect of a changing θ_B on the uniformity of the magnetic field magnitude over the length of the vapor cell when on axis ($x = 0$, $y = 0$, $z = z'$) for the two methods. Although not shown graphically here, we find that $|B|$ is much more uniform over the length of the vapor cell using the solenoid-plus-permanent method; for example, along ($x = 0$,

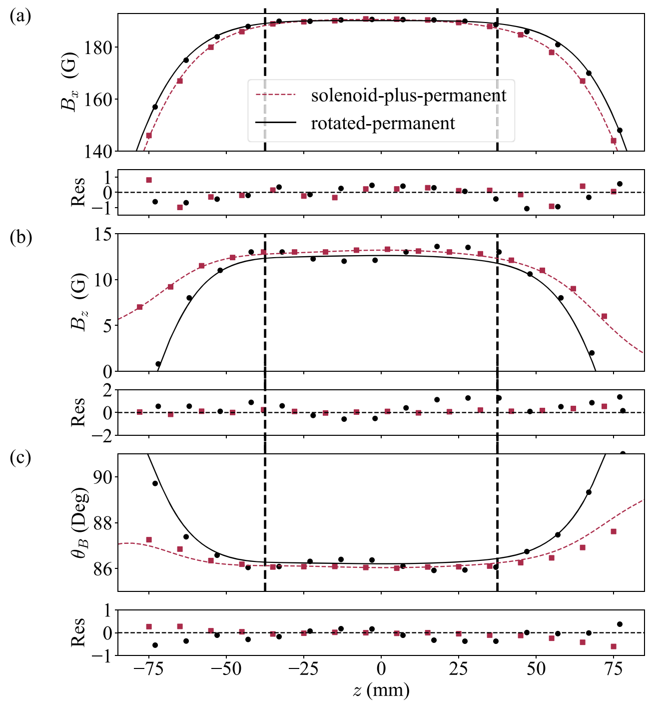

FIG. 5. Comparison of measured magnetic field components: (a) the transverse magnetic field (B_x) is plotted for the two different methods: solenoid-plus-permanent (red squares) and rotated-permanent (black circles). The theoretical model for each configuration is shown as a black solid line (rotated-permanent geometry) and a red dashed line (solenoid-plus-permanent). The two methods produce similar, uniform fields of 190 G over the position of the vapor cell, which is indicated by vertical black dashed lines. (b) The axial magnetic field (B_z) is plotted for the same configurations and has a value of 13 G over the length of the vapor cell. (c) θ_B, the angle of the magnetic field vector with respect to the z-axis. This is calculated from the measurements in (a) and (b). In both configurations, θ_B is ~86°. Residuals are shown below each subplot, illustrating an excellent agreement between the measured data and the theoretical model predictions.[55]

$y = 0$, $z = z'$), within the vapor cell, and at $\theta_B = 80^\circ$, the difference between the maximum and minimum magnetic field magnitudes of the solenoid-plus-permanent configuration was 2.5 G, whereas for the rotated-permanent configuration it was 10 G.

IV. RESULTS

We compare the two methods of generating the arbitrary-angle magnetic field through two approaches: first, by measuring the axial and transverse magnetic fields using a Hall probe; and second, by utilizing the atoms as magnetic field sensors within the magneto-optical filter.

A. Hall probe measurements

A transverse Hall probe (Magnetic Instruments GM08 Gaussmeter) was employed to measure the transverse field component, B_x, along the axis of the laser beam (z-axis). Figure 5(a) shows two experimentally measured field profiles (data points) as a function of z: the rotated-permanent geometry (black) and the solenoid-plus-permanent (red). Theoretical field profiles, calculated with *Magpylib*, are represented by solid or dashed lines in the corresponding colors. Notably, the maximum measured transverse magnetic field of the two configurations was the same, at 190 G over the region occupied by the vapor cell, as indicated by the dashed black lines. There is a small discrepancy between the field homogeneity of the two configurations: for the solenoid-plus-permanent configuration, the B_x root-mean-square (rms) variation is 1.5%, whereas for the rotated-permanent configuration, it is 0.7%. Irrespective of this, the residuals show excellent agreement between the data and the *Magpylib* model.

The axial magnetic field component B_z was measured using an axial Hall probe, and the results are depicted in Fig. 5(b). The results show good agreement between the two methods. For both, the maximum measured value of the field was 13 G, as expected. The field rms variation along ($x = 0$, $y = 0$, $z = z'$) is less than 4% over the length of the vapor cell for the solenoid-plus-permanent magnet configuration, whereas for the rotated-permanent configuration, the field rms variation is 13%. Residuals show excellent agreement between the experimental measurements and theoretical predictions. Again, the uniformity of the magnetic field along the length of the vapor cell was confirmed.

The magnetic field angle, θ_B, for the two configurations was calculated from the B_x and B_z using $\tan^{-1}(B_x/B_z)$ and is depicted in Fig. 5(c). θ_B is ~86° for both geometries, with a rms variation of 0.2° for the solenoid-plus-permanent configuration and 0.6° for the rotated-permanent configuration. The magnetic field magnitude, $|B|$, was calculated using $|B| = \sqrt{(B_x)^2 + (B_z)^2}$. For both configurations, $|B|$ is ~190 G with an rms variation of 1.5 and 0.7% for the solenoid-plus-permanent and rotated-permanent configurations, respectively.

The variations in the transverse and axial fields are likely attributed to the slight inhomogeneity of each individual magnet within the device. While the transverse and axial fields exhibit individual variations of over 1% on axis ($x = 0$, $y = 0$, $z = z'$)—a prerequisite of good magneto-optical filter performance as outlined in the introduction—it is crucial to note that the decisive factors influencing magneto-optical filter performance are the magnetic field magnitude and angle (assuming all other filter parameters remain constant). The rms variation of the magnetic field angle and magnitude are considered inconsequential in this study. This is due to the filter profile near the optimal θ_B being largely insensitive to small angle changes within 0.5°, as illustrated in Fig. 7.

We confined our Hall probe measurements of the axial and transverse magnetic fields to the central axis ($x = 0$, $y = 0$, $z = z'$) given that the laser beam width (in x and y) used in our magneto-optical filter typically spans ~1 mm. However, across a region where $+5$ mm $> x > -5$ mm ($y = 0$, $z = 0$), the *Magpylib* model indicates a 3% rms variation in the magnetic field magnitude for both configurations. Simultaneously, the rms variation of θ_B is 0.2° for the solenoid-plus-permanent configuration, while it is less than 0.1° for the rotated-permanent configuration. Again, these rms variations in magnetic field angle and magnitude are considered insignificant in this study.

B. Magneto-optical filter measurements

The results presented in Sec. IV A indicate minimal discrepancies in the magnetic field strength and angle between the two

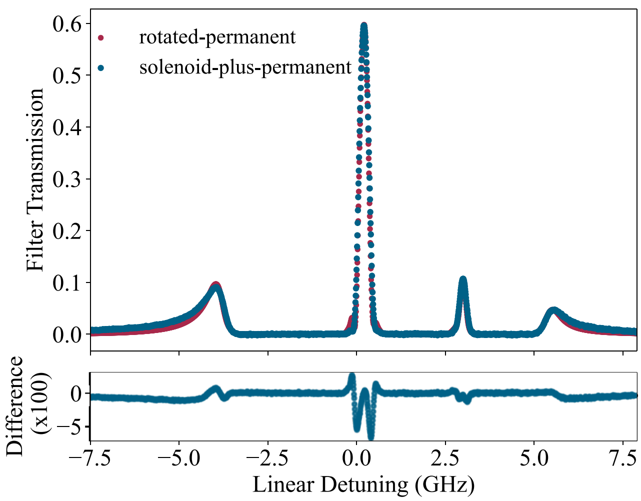

FIG. 6. Comparison between rotated-permanent (red points) and solenoid-plus-permanent (blue points) filter profiles. Both are for a natural abundance of Rb D2 transitions through a 75 mm vapor cell in the weak probe regime as a function of linear detuning. Plotted underneath are the differences between the two experiments, which show excellent agreement.

magnetic field configurations. Therefore, we expect the magneto-optical filter transmission profiles realized with the two configurations to be very similar. In this section, we construct magneto-optical filters with both field configurations and compare their profiles. In addition, we tune the angle of the magnetic field by changing the current in the solenoid.

Figure 6 compares the performance of the arbitrary-angle magnetic field filter produced by the rotated-permanent geometry with that produced using a solenoid-plus-permanent setup. The difference between the two profiles is shown in the bottom subplot. We see that there is excellent agreement between the two methods of producing the arbitrary magnetic field angle, with both methods producing all of the expected transmission features.[36] There is a slight disagreement between the two methods at the edges of the center transmission peak; this is due to the narrowness of the filter transmission profiles. The filter profiles were obtained in two separate experimental runs, whereby the magnetic environment the atoms reside in at the time of the experiment is different. This makes the data processing of the filter profiles sensitive to minor variations such as linearization, normalization, small angle differences, or magnetic field discrepancies between datasets.[45]

The solenoid offers an additional benefit by providing us with more efficient and rapid tuning capabilities. In contrast to the rotated-permanent configuration, where rotating the magnets to generate the arbitrary-angle magnetic field can be a slow process, we can swiftly adjust the magnetic field angle by simply changing the current supplied to the solenoid. The solenoid method also makes precisely selecting the angle easier, as this fine tuning is difficult when rotating permanent magnets by hand. This enhances the versatility and responsiveness of our experimental setup.

Figure 7(a) demonstrates the diverse filter spectra generated using the solenoid-plus-permanent configuration with varying current, as well as the effect on filter characteristics. The dark blue trace

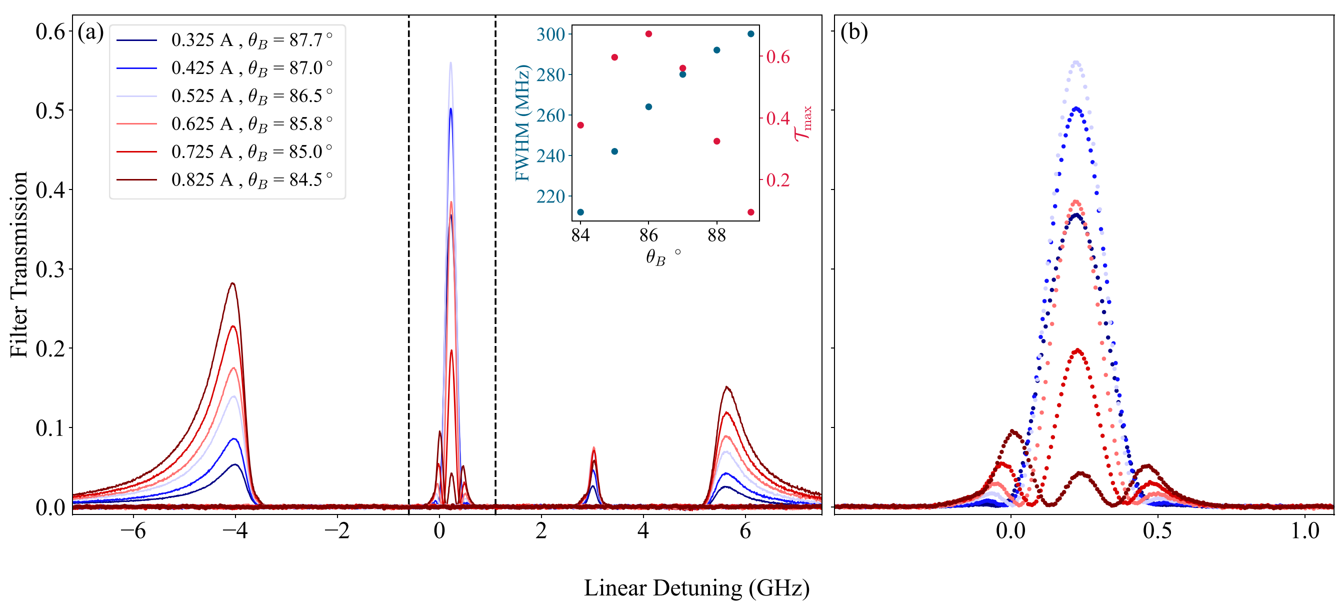

FIG. 7. (a) Experimental Rb D2 line magneto-optical filter transmission through a natural abundance Rb vapor cell of length l = 75 mm as a function of linear detuning in the weak probe regime. The plot shows the effect of changing solenoid current and, correspondingly, the angle, θ_B, of the total magnetic field, on the filter spectra with the solenoid-plus-permanent configuration. Quoted angles are extracted from *ElecSus* fits. (b) Shows an expanded view of the central peaks of the spectra. The inset shows theoretical predictions from *ElecSus* of the behavior of the full-width-at-half-maximum (FWHM) and the maximum transmission of the central filter peak as the magnetic field angle is varied.

shows the filter spectrum when a current of 0.325 A is applied to the solenoid. Increasing the solenoid current increases not only the height of the central peak but also the height of the other peaks. However, once the current reaches 0.625 A (i.e., θ_B = 85.8), an interesting change occurs: the transmission of the central peak starts to decrease, while the peaks at the wings continue to rise as expected from the theory.[37] A zoom in to the central region of the filters, as shown in Fig. 7(b), highlights the response of the main peak to varying currents. We also note that as the current increases, the main peak width increases continually. This central peak height and width behavior with changing angle, θ_B, is shown in the inset in Fig. 7.

The sensitivity of the magneto-optical filter response to a small angle change further reinforces why the solenoid-plus-permanent configuration is better suited for optimizing magneto-optical filters compared to using the rotated-permanent approach since the angle can be precisely controlled. Indeed, the solenoid-plus-permanent configuration has recently been used to demonstrate the magneto-optical filter with the highest recorded figure of merit to date.[50] Figure 7(b) demonstrates that a large change in peak transmission can be achieved by a small angular change in the direction of the magnetic field; this has the potential to be the basis of an optical switch.[51,52]

The largest angle solenoid-plus-permanent filter created and analyzed here had θ_B of 84.5°. However, the equipment used in this work has been used to produce an angle of θ_B = 66°. This value is limited by the chosen solenoid characteristics and the power supply. Larger B_z and correspondingly smaller θ_B could easily be produced using a different solenoid/power supply combination. Indeed, solenoids have been used to generate fields exceeding 4 kG in magneto-optical filter experiments, although this requires water cooling.[22] It would, therefore, be possible to create a solenoid-permanent magnet setup capable of producing any chosen field orientation. It should be noted, however, that in the case of large magnetic field angles using this setup, the resultant field magnitude is highly dependent on the field angle.

This wide range of achievable angles is in contrast to the rotated-permanent configuration, which has a physical limit (for our chosen magnets) of 70°, although the field-non-uniformity over the cell is a limiting factor well before this angle is reached.

V. CONCLUSION

In this study, we proposed a new method for generating an arbitrary magnetic field angle by combining a fixed Voigt geometry permanent magnet pair with a solenoid. This method allows for more precise and flexible control of the magnetic field angle than the previously used method of rotating the permanent magnet pair. To replicate the field produced by a rotated permanent magnet pair with our new method, we simulated the magnetic fields produced by both methods with *Magpylib*. Using these simulations, we were able to select appropriate solenoid-plus-permanent magnet parameters such that the old and new methods could be directly compared. Experimental analysis showed excellent agreement with comparable magnetic field strengths, angles, and magneto-optical filter profiles between both methods. The main limitations of the rotated-permanent method are the difficulty of selecting the rotated angle accurately and swiftly. In addition, the use of an extended vapor cell (to achieve better filter performance) causes difficulties, restricting the angular range achievable with the permanent magnet arbitrary-angle filter setup. These problems are resolved in the solenoid-plus-permanent configuration because the permanent magnets remain fixed relative to the cell. Therefore, larger angles can be created, and longer vapor cells can be used with this method, which will allow for better magneto-optical filters to be realized.[36] In addition, in the solenoid-plus-permanent configuration, we can adjust the magnetic field angle by simply changing the current supplied to the solenoid, which leads to fine-tuning of the rotated angle. We also show how small changes in magnetic field angle can create vastly different filter profiles, which the precise angle control and flexibility of our new design make easier to exploit.

ACKNOWLEDGMENTS

We gratefully acknowledge Steven Wrathmall and Liam Gallagher for helpful discussions and EPSRC (Grant No. EP/R002061/1) and the UK Space Agency (Grant No. UKSAG22_0031_ETP2-035) for funding. Sharaa Alqarni acknowledges Najran University, Najran, KSA (Grant No. 443-16-4151), for the financial support. We also acknowledge the constructive feedback from the anonymous referee.

AUTHOR DECLARATIONS

Conflict of Interest

The authors have no conflicts to disclose.

Author Contributions

Sharaa.A. Alqarni: Data curation (equal); Formal analysis (equal); Investigation (equal); Visualization (equal); Writing – original draft (equal); Writing – review & editing (equal). **Jack D. Briscoe**: Software (equal). **Clare R. Higgins**: Formal analysis (equal); Software (equal); Visualization (equal); Writing – review & editing (equal). **Fraser D. Logue**: Conceptualization (equal); Software (equal); Writing – review & editing (equal). **Danielle Pizzey**: Conceptualization (equal); Investigation (equal); Supervision (equal); Visualization (equal); Writing – review & editing (equal). **Thomas G. Robertson-Brown**: Investigation (equal); Software (equal). **Ifan G. Hughes**: Funding acquisition (equal); Project administration (equal); Supervision (equal); Writing – review & editing (equal).

DATA AVAILABILITY

The data that support the findings of this study are freely available in DRO at https://doi.org/10.15128/r2rb68xb893.[53]

REFERENCES

[1] D. Dick and T. M. Shay, Opt. Lett. **16**, 867 (1991).
[2] H. Chen, P. Searcy, E. Korevaar, and C. Y. She, Opt. Lett. **18**, 1019 (1993).
[3] P. Yeh, Appl. Opt. **21**, 2069 (1982).
[4] J. A. Zielińska, F. A. Beduini, N. Godbout, and M. W. Mitchell, Opt. Lett. **37**, 524 (2012).

[5] M. A. Zentile, D. J. Whiting, J. Keaveney, C. S. Adams, and I. G. Hughes, Opt. Lett. **40**, 2000 (2015); arXiv:1502.07187.
[6] I. Gerhardt, Opt. Lett. **43**, 5295 (2018).
[7] F. D. Logue, J. D. Briscoe, D. Pizzey, S. A. Wrathmall, and I. G. Hughes, Opt. Lett. **47**, 2975 (2022).
[8] Y. Ohman, Stock. Obs. Ann. **19**, 3 (1956).
[9] M. Cimino, A. Cacciani, and N. Sopranzi, Sol. Phys. **3**, 618 (1968).
[10] A. Cacciani and M. Fofi, Sol. Phys. **59**, 179 (1978).
[11] A. Cacciani, D. Ricci, P. Rosati, E. Rhodes, E. Smith, S. Tomczyk, and R. Ulrich, Il Nuovo Cimento C **13**, 125 (1990).
[12] R. Erdelyi, M. B. Korsos, X. Huang, Y. Yang, D. Pizzey, S. A. Wrathmall, I. Hughes, M. Dyer, V. S. Dhillon, B. Belucz, R. Brajsa, P. Chatterjee, X. Cheng, Y. Deng, S. V. Dominguez, R. Joya, P. Gomory, N. G. Gyenge, A. Hanslmeier, A. Kucera, D. Kuridze, F. Li, Z. Liu, L. Xu, M. Mathioudakis, S. Matthews, J. McAteer, A. A. Pevtsov, W. Potzi, P. Romano, J. Shen, J. Temesvary, A. G. Tlatov, C. Triana, D. Utz, A. M. Veronig, Y. Wang, Y. Yan, T. Zaqarashvili, and F. Zuccarello, J. Space Weather Space Climate **12**, 2 (2022) © 2021 The author(s). This is an author-produced version of a paper subsequently published in Journal of Space Weather and Space Climate. Uploaded in accordance with the publisher's self-archiving policy.
[13] C. Fricke-Begemann, M. Alpers, and J. Höffner, Opt. Lett. **27**, 1932 (2002).
[14] A. Popescu, K. Schorstein, and T. Walther, Appl. Phys. B **79**, 955 (2004).
[15] Y. Yang, X. Cheng, F. Li, X. Hu, X. Lin, and S. Gong, Opt. Lett. **36**, 1302 (2011).
[16] J. Keaveney, W. J. Hamlyn, C. S. Adams, and I. G. Hughes, Rev. Sci. Instrum. **87**, 095111 (2016).
[17] P. Chang, H. Shi, J. Miao, T. Shi, D. Pan, B. Luo, H. Guo, and J. Chen, Appl. Phys. Lett. **120**, 141102 (2022).
[18] T. Shi, X. Guan, P. Chang, J. Miao, D. Pan, B. Luo, H. Guo, and J. Chen, IEEE Photonics J. **12**, 1503211 (2020).
[19] Z. Liu, X. Guan, X. Qin, Z. Wang, H. Shi, J. Zhang, J. Miao, T. Shi, A. Dang, and J. Chen, arXiv:2301.01614 (2023).
[20] M. Faraday, Philos. Trans. R. Soc. London **136**, 1 (1846).
[21] S. D. Harrell, C.-Y. She, T. Yuan, D. A. Krueger, H. Chen, S. Chen, and Z. Hu, J. Opt. Soc. Am. B **26**, 659 (2009).
[22] W. Kiefer, R. Löw, J. Wrachtrup, and I. Gerhardt, Sci. Rep. **4**, 6552 (2014).
[23] W. Voigt, Ann. Phys. **303**, 345 (1899).
[24] F. S. Ponciano-Ojeda, F. D. Logue, and I. G. Hughes, J. Phys. B: At., Mol. Opt. Phys. **54**, 015401 (2020).
[25] F. Schuller, M. J. D. Macpherson, D. N. Stacey, R. B. Warrington, and K. P. Zetie, Opt. Commun. **86**, 123 (1991).
[26] M. W. Kudenov, B. Pantalone, and R. Yang, Appl. Opt. **59**, 5282 (2020).
[27] J. Menders, P. Searcy, K. Roff, and E. Korevaar, Opt. Lett. **17**, 1388 (1992).
[28] L. Yin, B. Luo, J. Xiong, and H. Guo, Opt. Express **24**, 6088 (2016).
[29] J. Keaveney, F. S. Ponciano-Ojeda, S. M. Rieche, M. J. Raine, D. P. Hampshire, and I. G. Hughes, J. Phys. B: At., Mol. Opt. Phys. **52**, 055003 (2019).
[30] T. Pyragius, H. M. Florez, and T. Fernholz, Phys. Rev. A **100**, 023416 (2019).
[31] K. Muroo, T. Matsunobe, Y. Shishido, Y. Tukubo, and M. Yamamoto, J. Opt. Soc. Am. B **11**, 409 (1994).
[32] J. D. Briscoe, F. D. Logue, D. Pizzey, S. A. Wrathmall, and I. G. Hughes, J. Phys. B: At., Mol. Opt. Phys. **56**, 105403 (2023).
[33] N. H. Edwards, S. J. Phipp, and P. E. G. Baird, J. Phys. B: At., Mol. Opt. Phys. **28**, 4041 (1995).
[34] G. Nienhuis and F. Schuller, Opt. Commun. **151**, 40 (1998).
[35] M. D. Rotondaro, B. V. Zhdanov, and R. J. Knize, J. Opt. Soc. Am. B **32**, 2507 (2015).
[36] J. Keaveney, S. A. Wrathmall, C. S. Adams, and I. G. Hughes, Opt. Lett. **43**, 4272 (2018).
[37] F. Logue , "Improving magneto-optical filter performance: Cascading and oblique B-fields," Ph.D. thesis, Durham University, 2023.
[38] C. R. Higgins, D. Pizzey, R. S. Mathew, and I. G. Hughes, OSA Continuum **3**, 961 (2020).
[39] D. J. Whiting, "Nonlinear optics in a thermal Rb vapour at high magnetic fields," Ph.D. thesis, Durham University, 2017.
[40] L. Weller, R. J. Bettles, P. Siddons, C. S. Adams, and I. G. Hughes, J. Phys. B: At., Mol. Opt. Phys. **44**, 195006 (2011).
[41] M. A. Zentile, J. Keaveney, R. S. Mathew, D. J. Whiting, C. S. Adams, and I. G. Hughes, J. Phys. B: At., Mol. Opt. Phys. **48**, 185001 (2015).
[42] M. Ortner and L. G. Coliado Bandeira, SoftwareX **11**, 100466 (2020).
[43] D. Pizzey, Rev. Sci. Instrum. **92**, 123002 (2021).
[44] M. Harris, S. Cornish, A. Tripathi, and I. Hughes, J. Phys. B: At., Mol. Opt. Phys. **41**, 085401 (2008).
[45] D. Pizzey, J. D. Briscoe, F. D. Logue, F. S. Ponciano-Ojeda, S. A. Wrathmall, and I. G. Hughes, New J. Phys. **24**, 125001 (2022).
[46] P. Siddons, C. S. Adams, C. Ge, and I. G. Hughes, J. Phys. B: At., Mol. Opt. Phys. **41**, 155004 (2008).
[47] M. A. Zentile, J. Keaveney, L. Weller, D. J. Whiting, C. S. Adams, and I. G. Hughes, Comput. Phys. Commun. **189**, 162 (2015).
[48] J. Keaveney, C. S. Adams, and I. G. Hughes, Comput. Phys. Commun. **224**, 311 (2018).
[49] B. E. Sherlock and I. G. Hughes, Am. J. Phys. **77**, 111 (2009).
[50] F. D. Logue, J. Briscoe, D. Pizzey, S. A. Wrathmall, I. G. Hughes *et al.*, arXiv:2303.00081 (2023).
[51] E. V. Raevsky and V. L. Pavlovitch, Opt. Eng. **38**, 1781 (1999).
[52] H Jelínková, J Šulc, P Koranda, M Němec, M Čech, M Jelínek, and V Škoda, "LiNbO3 Pockels cell for Q-switch of Er: YAG laser," Laser Physics Letters 1(2), **59** (2004).
[53] S. A. Alqarni, "A device for magnetic-field angle control in magneto-optical filters using a solenoid-permanent magnet pair [dataset]," Durham University Collections, 2023, https://doi.org/10.15128/r2rb68xb893.
[54] J. Keaveney, *Collective Atom–Light Interactions in Dense Atomic Vapours* (Springer, 2014).
[55] I. Hughes and T. Hase, *Measurements and Their Uncertainties: A Practical Guide to Modern Error Analysis* (Oxford University Press, Oxford, 2010).